

Coherent interaction-free detection of noise

John J. McCord,^{1,2} Shruti Dogra,^{1,2} and Gheorghe Sorin Paraoanu^{1,2}

¹*QTF Centre of Excellence, Department of Applied Physics, Aalto University, FI-00076 Aalto, Finland*

²*InstituteQ at Aalto University, FI-00076 Aalto, Finland*

(Dated: December 29, 2023)

Noise is an important concept and its measurement and characterization has been a flourishing area of research in contemporary mesoscopic physics. Here we propose interaction-free measurements as a noise-detection technique, exploring two conceptually different schemes: the coherent and the projective realizations. These detectors consist of a qutrit whose second transition is coupled to a resonant oscillatory field that may have noise in amplitude or phase. For comparison, we consider a more standard detector previously discussed in this context - a qubit coupled in a similar way to the noise source. We find that the qutrit scheme offers clear advantages, allowing precise detection and characterization of the noise, while the qubit does not. Finally, we study the signature of noise correlations in the detector's signal.

I. INTRODUCTION

The main obstacle to realizing large-scale quantum computers is noise, which hinders the realization of high-fidelity gates and readout [1–3]. The only known solution to this problem is quantum error correction, which requires however precise knowledge on the type of noise acting on the system. Phase noise is also an important factor for another quantum technology: it affects the quantum bit error rate in cryptography protocols based on weak coherent states, for example twin-field quantum key distribution [4] that can be in principle implemented also in the microwave range. Thus, diagnosing various sources of noise and the errors they produce is of utmost importance for the success of fault-tolerant quantum computing [5]. Noise is also an important source of information for the dynamics of electrons at the nanoscale, as summarized by the famous dictum of Landauer “noise is the signal” [6].

Since the noise itself depends strongly on the local micro-scale electromagnetic environment, a natural idea would be to use the qubits themselves as detectors of noise. Indeed, it has been noticed that qubits are in principle suitable devices as detectors of noise, since in the first-order perturbation theory the excitation and decay probabilities are proportional to the noise spectral density at the negative respectively positive qubit frequency [7]. This strategy has been also used successfully in magnetometry, where Ramsey interferometry with superconducting qubits has been used as a sensitive tool for measuring magnetic fields. [8–10]. Several techniques have been proposed, for example using dynamical decoupling and its filtering properties to reconstruct the power spectrum density [11, 12], using the qubit as a vector network analyzer for characterizing the control lines [13], identifying long-range correlations and reconstruction of the error rates observed experimentally [14], methods for characterization of low-frequency noise, whose correlations can be obtained by repeated Ramsey measurements [15], the use of spectator qubits and machine learning to monitor the noise in quantum processors [16]. In explor-

ing the dynamics of electronic transport, significant effort has been put into detectors sensitive to the full counting statistics: qubit-based detectors could be used for measuring the characteristic function by performing Ramsey measurements at different values of the coupling [17] or for extracting the third cumulant from changes in their effective temperature[18].

Here we focus on the detection of oscillator noise, a paradigmatic type of noise which becomes relevant especially in quantum control - when attempting to drive resonantly quantum systems which in general may interfere with the intended operations and lead to errors. We discuss both amplitude and phase noise. We exploit a recent [19, 20] coherent interaction-free measurement (cIFM) protocol for the detection of resonant noise in microwave circuits. This scheme is based on a three-level quantum system (qutrit) whose basis states are labeled as $|0\rangle, |1\rangle, |2\rangle$, and the allowed transition between levels $|0\rangle - |1\rangle$ and levels $|1\rangle - |2\rangle$ correspond to transition frequencies: ν_{01} and ν_{12} respectively. As per cIFM protocol, there is a train of identical beam-splitter unitaries targeting the $|0\rangle - |1\rangle$ transition, with its consecutive blocks being separated by a fixed duration. In-between each pair of beam-splitter unitaries, $|1\rangle - |2\rangle$ microwave pulses, called B -pulses may be sandwiched; whose presence is ascertained in an interaction-free manner [19, 20]. There are three possible outcomes of the protocol which leave the three-level system in one of the basis states ($|0\rangle, |1\rangle, |2\rangle$) with respective occupation probabilities: p_0, p_1 , and p_2 . For a qutrit being initialized in its ground state ($|0\rangle$), and undergoing cIFM protocol, one can have a successful interaction-free detection of B -pulse with probability p_0 , a non-desirable non-interaction-free detection with a probability p_2 and inconclusive results with probability p_1 . These probabilities have a direct correspondence with the populations of the respective energy levels of the qutrit. A different interaction-free concept, which we call projective interaction-free measurement, interjects projective measurements on state $|2\rangle$ after each interaction with the microwave B -pulses [20]. Projective interaction-free measurements have been performed in various quantum-optics experiments that fol-

lowed the original theoretical proposal. The projective measurement needed can be implemented as well in circuit quantum electrodynamics, for example by employing the switching of a Josephson junction when one of the excited states in the washboard potential is close to being delocalized [21–23]. For non-random pulses the coherent protocol turns out to be more efficient. Furthermore, it has been shown that coherent protocol reaches the Heisenberg limit when the Fisher information is evaluated at small strengths of the pulses-to-be-detected; whereas the projective protocol only reaches the standard quantum limit [20].

To understand the advantage of interaction-free measurements, we consider for comparison a paradigmatic detector based on absorption, consisting of a single qubit interacting resonantly with the field. The simplest detection scheme is to allow a qubit with transition frequency to evolve under this noise and read the qubit's state after some time. If the noise field has reasonably strong coupling with the detector qubit, then the state of the qubit will be influenced in the presence of noise. Therefore, a qubit initialized in its ground state $|g\rangle$ exhibits non-zero probability to be found in its excited state ($|e\rangle$). Thus one can use excited state population p_e as a marker to ascertain the presence of noise. This mechanism might seem simple and useful at first, but this is not so reliable in practice. Detector qubit evolves randomly under the influence of this noise leading to arbitrarily varying outcomes depending upon the qubit-noise coupling. Moreover, if the noisy signal sums arbitrarily close to zero in a given time, the detector qubit will not be able to detect the noise.

To study noise in a systematic manner, we consider a drive acting resonantly on the second 1-2 transition (in the case of cIFM and pIFM) or on the $g-e$ qubit transition. Noise can appear either in the amplitude or in the phase of the drive. If the correlation time of the noise is much larger than the total duration T of the sequence plus the measurement time, the problem of characterizing the noise is trivial, since each nearly-constant value of the drive can be detected with high efficiency. The interesting situation, which we consider in this work, is when the correlation time is much larger than τ_B and much smaller than T . This allows us to sample the noise in small τ_B intervals where it is nearly constant. This arrangement requires, ideally, that N is very large, while in real experiments N is limited by decoherence.

The paper is organized as follows: in Section II we introduce the three detector models - the qubit and the two interaction-free protocols utilizing the qutrit. We present our main results in Section III. In Section IV we discuss the case of binary noise describe by a Poissonian probability distribution. In Section V we examine the signatures of autocorrelations in the detector output. We conclude in Section VI.

II. DETECTOR MODELS

In the following subsections, we describe systematic and efficient techniques to detect resonant noise, exploiting qutrit-based protocols. Further, we compare the efficacies of these qubit-based and qutrit-based models to detect noise, highlighting the difference between absorptive and interaction-free measurements. In both cases we start with a generic oscillatory noisy signal $\Omega(t) = \Omega_0(t) \cos[\omega_0 t + \chi(t)]$ at a frequency ω_0 , which is coupled resonantly into the corresponding transition with a generic Rabi coupling Ω_0 . The phase $\chi(t)$ is in general noisy, and also we can separate a noisy component $\zeta(t)$ in the Rabi coupling $\Omega_0(t) = \Omega_0 + \zeta(t)$. As we shall see, the successful detection is established when the population p_e on the excited state $|e\rangle$ (for the qubit) or the population p_0 of the ground state $|0\rangle$ for the qutrit is nearly 1. Finding the detector in these respective states is therefore highly indicative for the presence of noise. We will refer to these probabilities generically as *marker populations*.

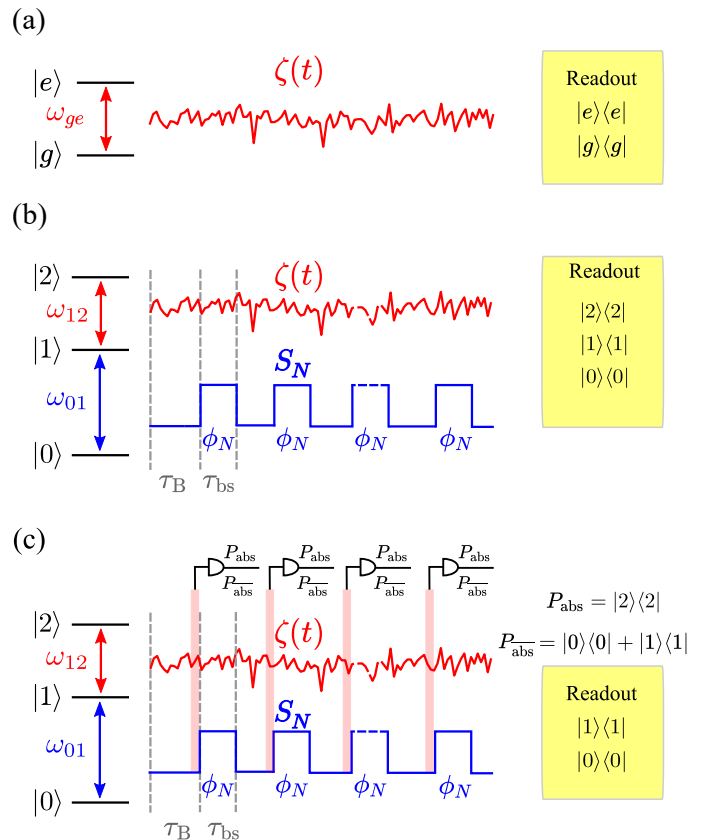


FIG. 1. The three noise detection schemes studied in this work: (a) qubit, (b) cIFM, and (c) pIFM.

A. Qubit-based detector

Consider a qubit with the computational basis denoted by ground and excited states $|g\rangle, |e\rangle$. The Hamiltonian under the drive is

$$H_{ge} = \hbar\omega_{ge}|e\rangle\langle e| + \hbar\Omega(t)\cos(\omega_0t + \chi(t))[|e\rangle\langle g| + |g\rangle\langle e|] \quad (1)$$

By introducing a unitary $U_{ge} = |g\rangle\langle g| + e^{i\omega_{ge}t}|e\rangle\langle e|$ we can transform this Hamiltonian into a frame rotating at the qubit frequency, $H_{ge} \rightarrow U_{ge}H_{ge}U_{ge}^\dagger + i\hbar(dU_{ge}/dt)U_{ge}^\dagger$ obtaining, in the rotating wave approximation and at resonance ($\omega_{eq} = \omega_0$)

$$H_{ge}(t) = \frac{\hbar\Omega_0(t)}{2} [e^{-i\chi(t)}|e\rangle\langle g| + e^{i\chi(t)}|g\rangle\langle e|] \quad (2)$$

$$= \frac{\hbar\Omega_0(t)\cos\chi(t)}{2}\sigma_{ge}^x - \frac{\hbar\Omega_0(t)\sin\chi(t)}{2}\sigma_{ge}^y \quad (3)$$

$$= \frac{\hbar\Omega_0(t)}{2}\hat{\mathbf{n}}_\chi(t)\sigma_{ge} \quad (4)$$

where $\sigma_{ge}^x = |g\rangle\langle e| + |e\rangle\langle g|$ and $\sigma_{ge}^y = -i|g\rangle\langle e| + i|e\rangle\langle g|$, $\sigma_{ge} = (\sigma_{ge}^x, \sigma_{ge}^y)$ and $\hat{\mathbf{n}}_\chi(t) = (\cos\chi(t), -\sin\chi(t))$ is a rotation axis in the xOy plane. In general, the Hamiltonian above does not commute with itself at different times. To deal with this issue, we divide the time into N intervals j of duration τ_B , during which $\chi(t)$ is approximately constant. In this case, the phase of the unitary transformation (φ) is same as the noise phase ($\chi(t)$). During these intervals, the unitary transformation produced by the pulses is

$$B(\theta_j) = e^{-i\theta_j\hat{\mathbf{n}}_j\sigma_{ge}/2} = \mathbb{I}_{ge}\cos\frac{\theta_j}{2} - i(\hat{\mathbf{n}}_j\sigma_{ge})\sin\frac{\theta_j}{2} \quad (5)$$

where $\theta_j = \int_{t_j}^{t_j+\tau_B}\Omega_0(t)dt = \Omega_0\tau_B + \int_{t_j}^{t_j+\tau_B}\zeta(t)dt$ is the arbitrary angle corresponding to the noisy drive [24], $\hat{\mathbf{n}}_j = (\cos\varphi_j, -\sin\varphi_j)$ is the axis of rotation, and \mathbb{I}_{ge} is the unit 2×2 matrix. Here t_j and $t_j + \tau_B$ are the initial and final times of the intervals.

In a more general situation the noise phase $\chi(t)$ varies significantly; in this case the unitary transformation of duration τ_B , effective angle θ_j , and an overall axis of rotation φ_j can be written as,

$$B(\theta_j) = e^{-i\theta_j\hat{\mathbf{n}}_j\sigma_{ge}/2} = \prod_{p=1}^{\mathcal{P}} e^{-i\delta\theta_p\hat{\mathbf{n}}_{\chi_p}\sigma_{ge}/2} \quad (6)$$

where $\delta\theta_p = \Omega_0(t)\delta t$ is the effective angle of rotation along the axis $\hat{\mathbf{n}}_{\chi_p}(t) = (\cos\chi_p(t), -\sin\chi_p(t))$ during p^{th} transient of duration δt . Here time (δt) is the infinitesimal time interval during which the noise amplitude $\zeta(t)$ and the noise phase $\chi(t)$ are approximately constant, which in the worst case, is the inverse of the noise sampling rate, and \mathcal{P} is the closest integer to $\tau_B/(\delta t)$.

B. Qutrit-based detector

Our models to detect noise using a qutrit with computational basis states ($|0\rangle, |1\rangle, |2\rangle$) are based on the cIFM and pIFM protocol, using which, we present an efficient detection of noise resonant with $|1\rangle - |2\rangle$ transition. In addition, a beam-splitter pulse of duration τ_{bs} is realized by coupling resonantly another field into the $|0\rangle - |1\rangle$ transition. The Hamiltonian under these drives is

$$H = \hbar\omega_{01}|1\rangle\langle 1| + \hbar(\omega_{01} + \omega_{12})|2\rangle\langle 2| + \quad (7)$$

$$\hbar\Omega_{01}(t)\cos(\omega_{01}t)[|1\rangle\langle 0| + |0\rangle\langle 1|] + \quad (8)$$

$$\hbar\Omega(t)\cos(\omega_0t + \chi(t))[|2\rangle\langle 1| + |1\rangle\langle 2|]. \quad (9)$$

With the unitary $U = |0\rangle\langle 0| + e^{i\omega_{01}t}|1\rangle\langle 1| + e^{i(\omega_{01}+\omega_{12})t}|2\rangle\langle 2|$ we can again transform this Hamiltonian into $H \rightarrow UH U^\dagger + i\hbar\frac{dU}{dt}U^\dagger$ and apply the rotating wave approximation under the resonance condition $\omega_0 = \omega_{01}$ to get

$$H(t) = \frac{i\hbar\Omega_{01}(t)}{2}[|1\rangle\langle 0| - |0\rangle\langle 1|] + \quad (10)$$

$$\frac{\hbar\Omega_0(t)}{2}[e^{-i\chi(t)}|2\rangle\langle 1| + e^{i\chi(t)}|1\rangle\langle 2|] \quad (11)$$

The protocol consists of a series of beam-splitter pulses of duration τ_{bs} on the 0-1 transition, intercalated with detection times τ_B onto which the noise is sensed. Introducing $\mathbb{I}_{kl} = |k\rangle\langle k| + |l\rangle\langle l|$, $\sigma_{kl}^y = -i|k\rangle\langle l| + i|l\rangle\langle k|$, $\sigma_{kl}^x = |k\rangle\langle l| + |l\rangle\langle k|$, with $k, l \in \{0, 1, 2\}$ and $k < l$ that are described by the unitary

$$S(\phi_N) = e^{-i\phi_N\sigma_{01}^y/2} \quad (12)$$

$$= \mathbb{I}_{01}\cos\frac{\phi_N}{2} - i\sigma_{01}^y\sin\frac{\phi_N}{2} + |2\rangle\langle 2| \quad (13)$$

Here the beam-splitter strengths ϕ_N are chosen such that $\phi_N = \pi/(N+1)$ by choosing appropriately the Rabi strengths $\phi_N = \int\Omega_{01}(t)dt$ corresponding to each pulse. Using again similar notations as for the qubit detector $\hat{\mathbf{n}}_k = (\cos\varphi_k, -\sin\varphi_k)$ when $\chi(t)$ is approximately constant for the duration τ_B *i.e.*, $\chi(t) = \varphi(t)$ and $\sigma_{12} = (\sigma_{12}^x, \sigma_{12}^y)$, or explicitly

$$B(\theta_k) = e^{-i\theta_k\hat{\mathbf{n}}_k\sigma_{12}/2} \quad (14)$$

$$= |0\rangle\langle 0| + \mathbb{I}_{12}\cos\frac{\theta_k}{2} - i(\hat{\mathbf{n}}_k\sigma_{12})\sin\frac{\theta_k}{2} \quad (15)$$

where the same definition for θ_k as in the qubit case applies. As in the qubit case, if $\chi(t)$ is not constant then, more generally, the effective unitary transformation for the duration τ_B takes a form similar to Eq. 6,

$$B(\theta_k) = \prod_{p=1}^{\mathcal{P}} e^{-i\delta\theta_p\hat{\mathbf{n}}_{\chi_p}\sigma_{12}/2} \quad (16)$$

a. Coherent IFM (cIFM) - based protocol As per the cIFM protocol, we have a train of beam-splitter unitaries

with frequency ν_{01} , each of them implementing a rotation of angle $\pi/(N+1)$ around the y axis, where $(N+1)$ is the total number of beam-splitter pulses. Each beam-splitter pulse is of duration τ_{bs} and consecutive beam-splitter pulses are separated from each other by time τ_B . In addition to these $|0\rangle - |1\rangle$ pulses, there is a noisy signal resonant at frequency $\nu = \nu_{12}$, which may be a continuous signal acting for a long time. We consider a smaller part of this noisy signal for a duration of $T = (N+1)(\tau_{bs} + \tau_B)$. We initialize our detector (qutrit) in state $|0\rangle$ and allow it to evolve with the series of beam-splitter unitaries in the presence of noise signal. Results from this protocol are read in a counter-intuitive manner *i.e.*, if no noise present, qutrit is found in state $|1\rangle$, while in the presence of noise, state of the qutrit remains the same ($|0\rangle$) with high probability. We use ground state probability (p_0) of the qutrit as a marker for the detection of noise. We obtain p_0 values at time T from several implementations with $N \in [1, 100]$. The whole process is then repeated a total of N_R times, and the average value of p_0 *i.e.*, $E[p_0]$ is observed.

b. Projective IFM (pIFM)-based model This is also a qutrit-based model to detect resonant noise. As described earlier, in pIFM-based model also there are $(N+1)$ beam-splitter unitaries of duration τ_{bs} , each implementing a rotation of angle $\pi/(N+1)$ around they axis. Similarly to the cIFM, the noise acts at the frequency $\nu = \nu_{12}$. Unlike the cIFM protocol where coherences are preserved as an asset to be used later, here coherences between levels $|1\rangle - |2\rangle$ are dropped via projective measurements at the end of each noise pulse implementation *i.e.*, at $T_i = (N_i + 1)(\tau_{bs} + \tau_B)$ where $N_i \in [0, N]$. Here also we use ground state population as marker, a non-zero value of which is the signature of noise.

III. RESULTS

We simulate qubit-based and qutrit-based detectors to ascertain the presence of resonant noise, considering different scenarios and comparing the corresponding results. Here we analyse the noise in three possible situations, (i) variation of $\zeta(t)$ at a constant phase *i.e.*, amplitude noise, (ii) variation of $\chi(t)$ with $\zeta(t)$ constant in time, *i.e.* phase noise, and (iii) a general case of both $\zeta(t)$ and $\chi(t)$ varying with time *i.e.* amplitude and phase noise. In all these cases, the noise signal is targeting only one specific frequency ω_{ge} (for the qubit case) or ω_{12} (for the qutrit case) and we divide this noise signal into several consecutive intervals of length τ_B and τ_{bs} . In the absence of simultaneous $|0\rangle - |1\rangle$ operations, the noise signal preceeding the i^{th} beam-splitter can be assumed as a unitary pulse $B(\theta_j)$ of duration τ_B , effective angle θ_j , and an overall axis of rotation φ_j . We assume that in the cIFM and pIFM protocols the three-level quantum system undergoes almost instantaneous beam-splitter operations, ensured by the condition $\tau_{bs} \ll \tau_B$. This produces a negligible er-

ror in the case of a continuous noise signal, where τ_{bs} is the time for which there exist simultaneous $|0\rangle - |1\rangle$ and $|1\rangle - |2\rangle$ drivings. Thus the sequence can be simplified to a series of beam-splitter unitaries and unitary pulses of arbitrary angles θ_j .

1. Amplitude noise

In the absence of simultaneous $|0\rangle - |1\rangle$ operations, the noise signal preceeding the i^{th} beam-splitter can be assumed as a unitary pulse of duration τ_B and effective angle $\theta_j = \Omega_0 \tau_B + \int_{t_j}^{t_j + \tau_B} \zeta(t) dt$ with fixed axis of rotation ($\chi = -\pi/2$ and hence $\varphi_j = -\pi/2$), where $t_j = N_j(\tau_{bs} + \tau_B)$ and $\tau_B + N_j(\tau_{bs} + \tau_B)$ are the initial and final times of each pulse, with $N_j \in [0, N]$.

For a relatively clear demonstration, we engineer a noisy signal with its net sum (for a long time) arbitrarily close to zero and the signal to noise ratio (SNR) being 1. To be more precise, in this case, we have $\sum_{j=1}^N \theta_j = 0$. The results obtained from this simple model are shown in Fig. 2(a,b). In Fig. 2(a), we present the mean value of the marker populations ($E[p_e]$ for the qubit and $E[p_0]$ for the qutrit), averaged over 500 replicas of the same experiment for various different values of $N \in [1, 100]$. Fig. 2(b) presents the corresponding values of variance for this state. Here, the continuous blue curve corresponds to the excited state population of the qubit-based detector, which is nearly zero; therefore the qubit detector misses completely the presence of noise. Further, the continuous red curve and the dashed black curve correspond to average value of p_0 resulting from cIFM and pIFM protocols respectively. In both of these cases, $E[p_0]$ approaches 1 for large N , signifying that both cIFM and pIFM based detectors are almost equally efficient in detecting noise in such scenarios.

In general the noise may not have its net sum approaching zero over a long time range ($\approx T$). In that case, the qubit detector will evolve with the net sum of the noise signal, such that $p_e = \sin^2(\theta_T)$, where $\theta_T = \sum_{i=1}^N \theta_i$. Thus the mean value, $E[p_e]$ approaches 0.5 after several repetitions, which is also consistent with the average value of $\sin^2(\theta_T)$ for $\theta_T \in [0, \pi]$. Such situations are shown in Fig. 2(c,e,g), which are discussed in the following subsections.

We also consider a situation with only positive values of noise *i.e.*, $\zeta_i(t) > 0$; we observe that the qubit detector leads to same outcome, which is expected. Interestingly, the pIFM based qutrit detector also has same outcomes, while cIFM protocol leads to improvement in the average values. In this case, cIFM protocol outperforms the pIFM protocol for the detection of positive resonant noise. pIFM is independent of the axis of rotation φ while cIFM is very sensitive to that. Thus we can acquire information about the phase φ from cIFM protocol but not from pIFM protocol. Next, we consider a situation with small values of $\theta_j \in [0, \pi/6]$ with $\varphi_j = -\pi/2$

as shown in Fig. 2(e,f). In this case, $E[p_0]$ from cIFM is already approaching 1 for $N > 20$, which is much better than pIFM, where $E[p_0] \approx 0.25$ for $N = 100$. The qubit initially oscillates at $\sin^2(\sum \theta_i)$ and finally attains the value 0.5.

2. Amplitude and phase noise

A more general noise signal may have time dependence for both its amplitude as well its phase. The results from this general scenario are shown in Fig. 2(c,d). As expected, the mean values in case of the qubit detector tend to stay close to 0.5. For strong enough noise signals, such that $\theta_i \in [0, \pi]$, both mean and variance values are independent of the value of N . In fact, the variance in p_1 values of a qubit has almost similar ranges when we plot it as a function of number of noise pulses (N) or the number of realizations (N_R). Thus we can conclude that due to quite large variance values, a widely varying output, and having a higher insensitivity, the qubit detector is less efficient.

We then allow the same noise signal to be accessed by the qutrit detectors, and the corresponding mean and variance values are shown with continuous red curve in case of cIFM and dashed black curve in case of pIFM in Fig. 2. For large values of N , the variance is quite close to zero and $E[p_0]$ is close to 1, signifying a very efficient detection of noise. Interestingly, continuous red and dashed black curves in Fig. 2(c,d) are not very different from that of Fig. 2(a,b). This demonstrates the efficiency of qutrit-based protocols irrespective of whether noise sums to zero or not.

3. Phase noise

Here we have a constant amplitude of noise such that $\theta = \pi/2$ and arbitrarily chosen phase, $\varphi \in [-\pi, \pi]$. The corresponding results are shown in Fig. 2(g,h). As expected, pIFM-based protocol is not sensitive to changes in φ , so its mean value marker is unchanged for any arbitrary value of φ , and hence the corresponding variance is zero. Clearly, it is not possible to characterize phase noise using pIFM-based detectors. While cIFM-based protocol is highly sensitive to the variations in φ and hence it can be more useful to infer the nature of noise. Qubit-based protocol is the least informative about noise, with its mean value staying close to 0.5 and significantly high values of variance. Also, the qubit-based protocol does not detect the presence of phase noise when θ is an integral multiple of π .

IV. DETECTION OF BINARY PROCESSES

In electronic and communication devices, it is common to come across shot noise, which is discrete in nature.

Here we consider shot noise as a binary noise signal and attempt to detect its presence via IFM-based protocols. We consider a Poisson point process leading to noise with steps $\pm\pi$,

$$p(m, T) = \frac{(\nu T)^m}{m!} e^{-\nu T}, \quad (17)$$

where $\nu = 1/\tau$ is the switching frequency. The correlation time τ is considered in such a way that $T \geq \tau > 0$, where $T = (N + 1)(\tau_b + \tau_{bs})$. The mean of the distribution $p(m, T)$ is $\lambda = \nu T = T/\tau$. Thus, as τ increases, the switching frequency decreases; correspondingly the mean and variance of the distribution decrease. An example of noise signal for time T with $\tau \in [\tau_{BS}, T]$, varying linearly in the given range and with noise amplitude of $\theta = \pm\pi$ is shown in Fig. 3. Here we analyse the case of a noise signal which can have its phase flipped at the rate of up to 10^9 times in one second *i.e.* a noise sampling rate of 1 G samples/s. We consider an intercept of such noise signal for a fixed duration of time T and try to detect it using cIFM and pIFM protocols. Fixing the values of $\tau_{BS} = 20$ ns and $T = 10$ μ s, we arbitrarily choose the value of $N \in [1, 40]$, *e.g.* $N = 1$ would mean placing two beam-splitter unitaries $((\pi/2)_y^{0-1})$; one in the beginning and one at the end of this noise signal, such that B-pulse duration, $\tau_B = T$. For an arbitrary value of N , we have $N + 1$ beam-splitter unitaries $((\pi/(N + 1))_y^{0-1})$ placed at intervals of $\tau_B = T/N$ on resonance with $|0\rangle - |1\rangle$ transition frequency, while the noise signal is acting on resonance with $|1\rangle - |2\rangle$ transition. Ideally, the protocol here is designed in such a way that the beam-splitter pulses should act instantaneously with $\tau_{BS} \rightarrow 0$, however due to the constraints by quantum speed-limit, and also for experimental feasibility, τ_{bs} is finite. The values of T , τ_{BS} , and N are chosen in such a way that even for the largest value of N , $\tau_{BS} \ll \tau_B$ and the qutrit's evolution under $|1\rangle - |2\rangle$ drive may be ignored during the short intervals τ_{BS} when the beam-splitter unitaries are acting in the $|0\rangle - |1\rangle$ subspace.

We consider the evolution of our detector qutrit under such noise (see Fig. 3) as per cIFM and pIFM protocols. When the noise sampling rate is much larger than N , cIFM and pIFM protocols give rise to similar results. For large enough $\theta \approx \pi$, these protocols are almost independent of τ with $E[p_0]$ almost constant for a wide range of τ . Further, for small enough values of N (≥ 10), $E[p_0]$ is already greater than 0.8. Therefore, in case of fast transiting and strongly coupled noise signal, cIFM or pIFM protocols are quite efficient to confirm the presence of noise signal even for small values of N . On the other hand, if this noise signal with $\theta = \pi$ is allowed to interact with a qubit on resonance, it is very likely for the qubit to not detect any noise at all as such noise signal is very likely to sum up to zero.

For relatively weakly coupled noise, from the cIFM protocol are shown in Fig. 5, where the left panels correspond to $\tau \in [0.01, 10]\mu$ s while the right panels present the results in a narrower range of $\tau \in [0.001, 0.1]\mu$ s. The

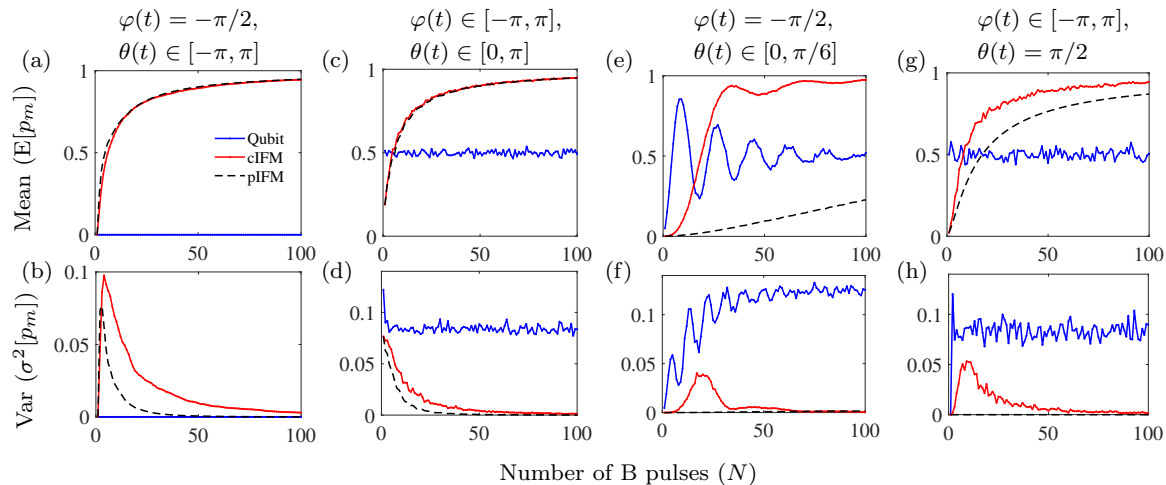


FIG. 2. Mean (top row) and variance (bottom row) of the marker populations (p_m) *i.e.*, p_e for qubit-based detector and p_0 for qutrit-based detectors, extracted from $N_R = 500$ realizations of the protocol, each with $\Omega_0 = 0$, and $N \in [1, 100]$. Panels (a), (b) correspond to the case of amplitude noise with net sum zero *i.e.*, $\sum_{j=1}^N \theta_j = 0$. Results from the general case of the $\zeta(t)$ is shown in panels (c) and (d), with both amplitude and phase noise. Panels (e),(f) correspond to the case of amplitude noise with small values of arbitrarily chosen θ . Panels (g), (h) show the results from phase noise at constant amplitude of the noise. The ranges of amplitude (θ) and phase (φ) are given at the top of each column.

top row shows the mean value of the ground state population $E[p_0]$ obtained from various realizations of the simulation; the corresponding standard deviations in the p_0 values are shown in the bottom row. Here $\theta = \pm\pi/4$, the noise sampling rate is 10^9 G samples/s, and $N \in [1, 40]$. So, for weakly coupled noise signals, the marker population p_0 assumes higher values for larger values of τ , which corresponds to the Poisson point process which has smaller mean and thus the switching frequency of the noise signal is relatively lower. These weaker noise signal also swiftly saturate the p_0 values for $\tau \geq 0.1\mu\text{s}$ and $N \geq 15$. Beyond a threshold τ , here also we observe that p_0 is almost independent of the correlation time. Therefore an optimal range of values of N and τ can be efficiently detected both via cIFM and pIFM protocols.

V. NOISE CORRELATIONS

The correlations present in the noise can often be used to reveal the underlying mechanism responsible for the fluctuations. In this section we first show how a qubit detector could be used to measure the full counting statistics of the noise. Then, we demonstrate that under certain conditions, correlations of random binary processes lead to different marker populations in the qutrit detectors.

A. Full counting statistics with a qubit detector

The problem of extracting the correlations of a random event is especially relevant in mesoscopic physics,

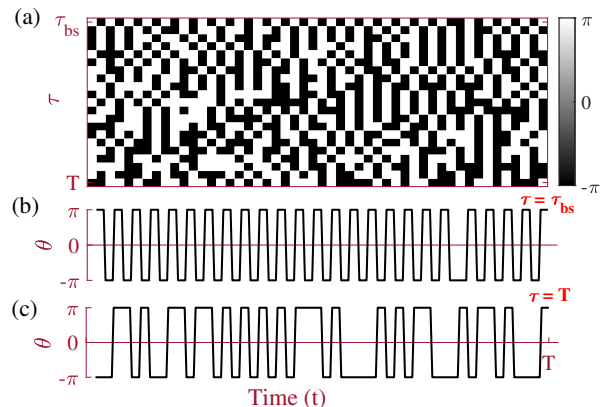


FIG. 3. Binary noise for time T , resulting from Poisson point process with mean $\lambda = T/\tau$, with correlation time length $\tau \in [\tau_{\text{BS}}, T]$. A complete matrix representation of one realization of this noise is shown in panel (a), while the 1-d traces shown in (b) and (c) correspond to two extreme values of the correlation time $\tau = \tau_{\text{BS}}$ and $\tau = T$ respectively.

where finding a way to measure the statistics of electronic transport in nanoelectronic devices led to the so-called problem of full counting statistics. In full counting statistics, we are interested in the probability distribution $P(m)$ of events m in a given time interval. The complete information about correlations is encapsulated into the so-called generating function, which allows us to calculate arbitrarily high-order cumulants associated with a probability distribution $P(m)$. The characteristic function is defined as the Fourier transform of $P(m)$. The compact variable of this transform (called counting field) can sometimes be understood as the coupling be-

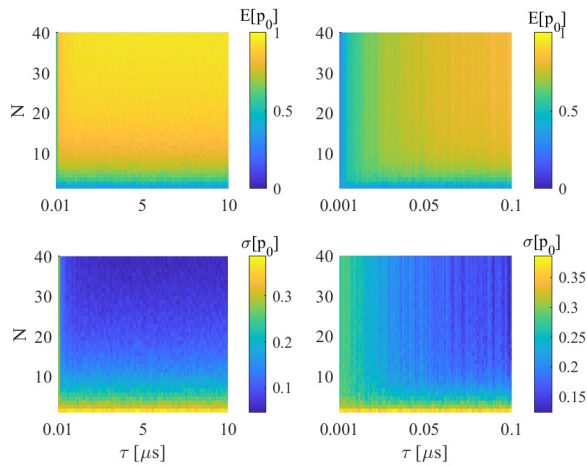


FIG. 4. The upper panels present the average of p_0 while the lower ones the standard deviations. The right panels show a narrower range of τ values compared to the left ones.

tween the noise and a detector. For example, in proposals that use a qubit to characterize the statistics of electrons transmitted through a quantum point contact, the counting field is the coupling between the current generated by the electrons and the σ_z operator of the qubit [17]. Here we consider the qubit detector, as described above, and we ask the question: given the cIFM protocol, what is the signature of higher-order cumulants of amplitude noise in the measured signal? In this case, a simple setup of the problem can be achieved by discretizing $\theta(t)$ in terms of θ , which can serve as the counting field and incorporates the physical dipole coupling between the noise and the detector. We consider the time interval of a full Ramsey sequence $T = \tau_{\text{bs}}(N + 1) + N\tau_{\text{B}}$ and we count how many times m we had a non-zero θ , with the total angle accumulated being $\theta_T = \int_0^T \Omega(t)dt = \sum_{i=1}^N \theta_j = m\theta$.

The generating function is then

$$\Lambda(\theta) = \langle e^{im\theta} \rangle = \sum_m P(m)e^{im\theta}. \quad (18)$$

from which the k -th order momenta M_k of m can be obtained by

$$M_k = \langle m^k \rangle = (-i)^k \lim_{\theta \rightarrow 0} \partial_\theta^k \Lambda(\theta). \quad (19)$$

For the qubit starting with the state $|0\rangle$ we get for the probability of ending up in the state $|1\rangle$

$$P_e(m\theta) = \frac{1}{2}(1 - \cos(m\theta)) \quad (20)$$

therefore

$$P_e(\theta) = \sum_m P(m) \frac{1}{2}(1 - \cos(m\theta)) = \frac{1}{2}(1 - \Re(\Lambda(\theta))) \quad (21)$$

In a similar way, starting with the state $(1/\sqrt{2})(|0\rangle + |1\rangle)$, we obtain

$$P_e(m\theta) = \frac{1}{2}(1 + \sin(m\theta)). \quad (22)$$

and therefore

$$P_e(\lambda) = \sum_m P(m) \frac{1}{2}(1 + \sin(m\theta)) = \frac{1}{2}(1 + \Im(\Lambda(\theta))). \quad (23)$$

This means that we can obtain directly both the real and imaginary part of the momentum generating function by measuring the probability P_e with two different initial conditions. We would then repeat this for various values of θ (which can be varied by tuning the coupling of the signal into the qutrit, by the use of attenuators, etc), obtain an approximate functional dependence $\Lambda(\theta)$, and extract the momenta using Eq. (19).

The full counting statistics offers a different perspective on characterizing noise than the usual analysis of correlation, by counting events in a time interval. The two perspective are, of course, connected to one another, although the relationship may not always be simple [25]. For example, if we fix the value of θ , the second-order momenta can be obtained as

$$\langle \theta_T^2 \rangle = M_2 \theta^2 = \int_0^T \int_0^T \langle \Omega(t_1)\Omega(t_2) \rangle dt_1 dt_2 \quad (24)$$

$$= T \int_{-\infty}^{\infty} \langle \Omega(0)\Omega(\tau) \rangle d\tau = T S_\Omega(f=0) \quad (25)$$

where the second row is obtained by a change of variables $T = (t_1 + t_2)/2$, $\tau = t_2 - t_1$ and T is assumed large.

B. Signatures of correlations in qutrit cIFM

In the previous subsection, we have seen that the response of the qubit does not depend on how the m occurrences of θ pulses are distributed in the time interval T : they would just sum up to $m\theta$ and the response would be a sine or cosine of $m\theta$. This is not the case for cIFM or pIFM, which are both sensitive to how these events are correlated. To illustrate this, consider a uniform distribution of θ values over the N τ_{B} -durations. In this case, for the cIFM, we have $S(\phi_N)[B(\theta)S(\phi_N)]^N|0\rangle$ as the final state and we can utilize the results for the probability amplitudes from Ref. [20]. Let us consider now the opposite situation: we concentrate all the driving power in one single interaction with the qutrit, occurring after the n 'th application of $S(\phi_N)$ ($0 < n < N$). We have as the final state $[S(\phi_N)]^{N+1-n}B(N\theta)[S(\phi_N)]^n|0\rangle = c_0|0\rangle + c_1|1\rangle + c_2|2\rangle$,

and we obtain the probability amplitudes

$$c_0 = \sin(n\phi_N) \sin^2 \frac{N\theta}{4} \quad (26)$$

$$c_1 = \cos^2 \frac{N\theta}{4} + \cos(n\phi_N) \sin^2 \frac{N\theta}{4} \quad (27)$$

$$c_2 = \sin \frac{N\theta}{2} \sin \frac{n\phi_N}{2} \quad (28)$$

In comparison with the uniform case, the differences are major. For example, increasing N at fixed m does not suppress the coefficient c_1 as in the uniform case. In fact, at large N we would get $c_0 \simeq 0$, $c_1 \simeq 1$, $c_2 \simeq 0$, so the signal produced is the same as for the case when no pulse is present. In other words, the detector misses completely the extremely strong $N\theta$ pulse.

This feature means that under certain conditions cIFM can distinguish between bunched noise signals and other arbitrarily-correlated noises. To illustrate this we simulate binary noise signals with amplitudes $\pm\pi$, assuming that the noise amplitude stays constant within a B-pulse duration. For an arbitrary value of N , we generate N events using the Poisson point process as described in Section IV with a noise sampling rate of $N\tau_B/T$ corresponding to different values of $\tau \in [10\text{ns}, T]$ and observe the ground state populations for different values of τ and N . The results are shown in Fig. 5 where upper panel (a) presents an example of binary noise signal for $N = 6$ at $\tau = \tau_{\min} = 10$ ns (left) and at $\tau = \tau_{\max} = 6\tau_b = 600$ ns (right). The mean value of the Poisson distribution ($\lambda = T/\tau$) is quite different in these two situations, which is reflected in the nature of these noise signals, despite the average value of θ , which is very likely to be the same for various values of τ . For larger τ , it is more likely to have less frequent switching of the noise amplitude and this case would lead to bunching of the noise pulses. Fig. 5(b), (c) present the mean value of p_0 obtained from several repetitions of the cIFM protocol as a function of correlation time τ . Different curves correspond to different values of N , as specified in the plot legends. As we go from left to right, the noise signal is more likely to have bunching which leads to a higher p_0 values. Note also that the larger N gets, the more insensitive the detection becomes to the underlying correlations of the noise.

VI. CONCLUSIONS

Characterizing noise at certain frequencies is essential for the development of quantum technologies. Here we show how, by using interaction-free measurements implemented with a qutrit, we can sense low-intensity random signals and also observe features that depend on the correlations. This is compared with the case of a single qubit used as a detector. The qubit is the simplest example of an absorption detector - where the noise creates an excitation that can be subsequently observed. In contrast, the interaction-free detection does not result in any excitations in the qutrit used as detector. We find that, for

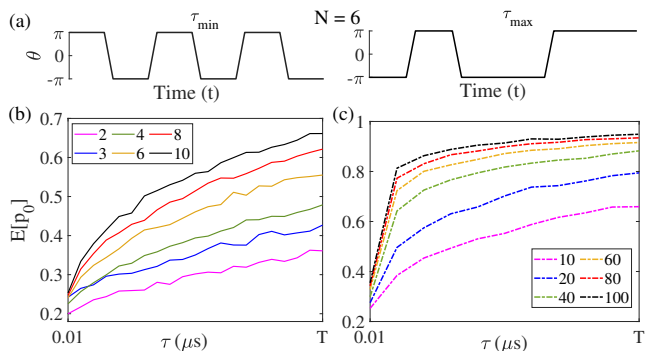


FIG. 5. (a) Illustration of a binary random process for $N = 6$ for two extreme values of the correlation time τ , where the trace on the right demonstrates bunching of the pulses. Panels (b) and (c) show the average of p_0 over 2000 realizations as a function of τ , with different curves corresponding to various different values of N .

a variety of types of noise, interaction-free measurements are much more effective. Our cIFM and pIFM protocols get more efficient with increasing N , which is evident from the increasing mean values and almost diminishing values of variance in the marker populations, which signify that only a few repetitions of the detection protocol should be enough to detect the presence of noise. Our results are general, with applicability on any experimental platform where interaction-free measurements can be implemented.

ACKNOWLEDGMENTS

We acknowledge financial support from Business Finland QuTI (decision 41419/31/2020) as well as from the Academy of Finland Centre of Excellence program (project 352925).

Appendix A: Noise characteristics

For completeness we give a brief presentation of the notations and concepts related to noise utilized here [26]. In general, for a random time-dependent variable $X(t)$ we define the two-sided power spectrum density at a frequency f as

$$S_X(f) = \int_{-\infty}^{\infty} R_{XX}(\tau) e^{-i2\pi f\tau} d\tau, \quad (\text{A1})$$

where $R_{XX}(\tau) = \mathbb{E}\{X(t)X(t+\tau)\}$. For ergodic processes the ensemble average is identical to the time-average, therefore $R_{XX}(\tau) = \lim_{T \rightarrow \infty} \frac{1}{T} \int_{-T/2}^{T/2} X(t)X(t+\tau) dt$. Moreover, the average power $\overline{X^2}$ can be obtained as $\overline{X(t)^2} = R_{XX}(0) = \int_{-\infty}^{\infty} S_X(f) df$. If $X(t)$ is a real random variable, then it follows directly from the definitions that both R_{XX} and $S_X(f)$ are even and real-valued. The

power spectral density can more conveniently be obtained from the windowed Fourier transform

$$X_T(f) = \int_{-T/2}^{T/2} dt X(t) e^{-i2\pi ft} \quad (\text{A2})$$

as

$$S_X(f) = \lim_{T \rightarrow \infty} \frac{1}{T} |X_T(f)|^2. \quad (\text{A3})$$

From here we see that $S_X(f)$ is also positive. Since in real experiments the frequency f is positive, it is convenient to introduce the single-sideband power spectrum density defined by $\mathbb{S}_X(f) = 2S_X(f)$ if $f > 0$ and zero otherwise.

In the case of a generic drive with nominal frequency ω_0 and Rabi coupling $\Omega(t)$ we can write $\Omega(t) \cos(\omega_0 t + \chi(t))$, where $\chi(t)$ is the phase noise. The Rabi coupling is also noisy, with associated double-sided spectral density

$$S_\Omega(f) = \lim_{T \rightarrow \infty} \frac{1}{T} |\Omega_T(f)|^2. \quad (\text{A4})$$

The double-sided spectral density of the phase noise is

$$S_\chi(f) = \lim_{T \rightarrow \infty} \frac{1}{T} |\chi_T(f)|^2 \quad (\text{rad}^2/\text{Hz}), \quad (\text{A5})$$

and on a logarithmic scale

$$\mathcal{L}(f) = 10 \log_{10}[S_\chi(f)] \quad (\text{dB}_c/\text{Hz}). \quad (\text{A6})$$

The fluctuations can also be characterized by the variance

$$\sigma_\chi = \sqrt{(\Delta\chi)^2} = \sqrt{\int_{-\infty}^{\infty} S_\chi(f) df} = \sqrt{\int_0^{\infty} \mathbb{S}_\chi(f) df}. \quad (\text{A7})$$

It is also convenient to introduce the fractional frequency noise, defined via the random variable $y(t) = \Delta\omega(t)/\omega_0$. Here $\Delta\omega(t) = \omega(t) - \omega_0$ and $\omega(t) = \frac{d}{dt}[\omega_0 t + \chi(t)] = \omega_0 + \dot{\chi}(t)$. Then the power spectrum density of the fractional frequency noise is

$$S_y(f) = \frac{(2\pi f)^2}{\omega_0^2} S_\chi(f). \quad (\text{A8})$$

Different power laws as a function of the frequency f can be obtained depending on the mechanism causing it, making one or another type of noise dominant at low, intermediate, or large frequencies. The most important types encountered in oscillators are as follows, in the order mentioned above: random walk of frequency ($S_y(f) \sim 1/f^2$, $S_\chi(f) \sim 1/f^4$), frequency flicker ($S_y(f) \sim 1/f$, $S_\chi(f) \sim 1/f^3$), random walk of phase or white noise of frequency ($S_y(f) \sim \text{const}$, $S_\chi(f) \sim 1/f^2$), phase flicker ($S_y(f) \sim f$, $S_\chi(f) \sim 1/f$), and white noise of phase ($S_y(f) \sim f^2$, $S_\chi(f) \sim \text{const}$).

Our protocol has been tested using different noise colors $\mathcal{N} \propto f^{-\alpha}$ and compared with the projective protocol using the same noise signatures. In particular, we have observed the success probabilities at different colors,

i.e. brown ($\alpha = 2$), pink ($\alpha = 1$), white ($\alpha = 0$), blue ($\alpha = -1$), and purple ($\alpha = -2$). Further, by looking at the power spectrum density (PSD) over these noise signatures and applying successive smoothing of the noise, we have extracted the leading coefficients a of the best-fit curve, which are found to be close to the expected values.

Appendix B: Comparison between cIFM and qubit-based protocols

To understand why cIFM is better than the qubit, consider the case $N = 2$. In this case S_2 is realized by a $\Phi_2 = \pi/3$ pulse and has the form

$$S_2 = \frac{\sqrt{3}}{2} \mathbb{I}_{01} - \frac{i}{2} \sigma_{01}^y + |2\rangle\langle 2|. \quad (\text{B1})$$

Let us assume now that the first B pulse has angle $\theta > 0$ while the second one has angle $-\theta$. For a qubit detector, this would result in a complete cancellation of the detection signal. However, in the case of cFM, the state after the application of the algorithm reads

$$\begin{aligned} & \left(\frac{3\sqrt{3}}{8} - \frac{2\sqrt{3}}{8} \cos \frac{\theta}{2} - \frac{\sqrt{3}}{8} \cos^2 \frac{\theta}{2} - \frac{1}{4} \sin^2 \frac{\theta}{2} \right) |0\rangle \\ & + \left(\frac{3}{8} + \frac{2}{8} \cos \frac{\theta}{2} + \frac{3}{8} \cos^2 \frac{\theta}{2} + \frac{\sqrt{3}}{4} \sin^2 \frac{\theta}{2} \right) |1\rangle \\ & + \left(\frac{2 - \sqrt{3}}{4} \sin \frac{\theta}{2} \cos \frac{\theta}{2} - \frac{\sqrt{3}}{4} \sin \frac{\theta}{2} \right) |2\rangle. \end{aligned} \quad (\text{B2})$$

One clearly sees that the amplitude probability for the state $|0\rangle$ is not zero. Even when $\theta \ll 1$ we can approximate the state as

$$-\frac{\theta^2}{16} |0\rangle + \left[1 + \frac{(2 + \sqrt{3})\theta^2}{16} \right] |1\rangle + \frac{\theta}{4} (1 - \sqrt{3}) |2\rangle, \quad (\text{B3})$$

and we can see that the amplitude for $|0\rangle$ is second order in θ but not zero.

Now, consider the general case of sampling the noise taking values of θ and $-\theta$ with equal probability using $N+1$ beam-splitter unitaries. If $N = 2$ as above, the sampling space consists of $(+\theta, +\theta)$, $(+\theta, -\theta)$, $(-\theta, +\theta)$, and $(-\theta, -\theta)$. The alternating-sign situations occurs with the same probability as the same-sign situations, therefore there is no clear advantage for cIFM. However, when N gets large, the number of cases in which the sum of $\theta_j = \pm\theta$'s is k , that is $\sum_{j=1}^N \theta_j = (N-k)\theta + k(-\theta) = (N-2k)\theta$ is determined by binomial coefficient C_k^N . Specifically, the probability distribution is the binomial one

$$p(k) = \frac{1}{2^N} C_k^N. \quad (\text{B4})$$

In the limit of large N this can be approximated by the normal distribution

$$p(k) = \frac{2}{\sqrt{\pi N}} e^{-2(k - \frac{N}{2})^2 / N}. \quad (\text{B5})$$

We can see that the maximum of p occurs at $k = N/2$, in which case $\sum_{j=1}^N \theta_j = 0$.

-
- [1] M. A. Nielsen and I. L. Chuang, *Quantum Computation and Quantum Information* (Cambridge University Press, Cambridge UK, 2002).
- [2] M. P. Silveri, J. A. Tuorila, E. V. Thuneberg, and G. S. Paraoanu, Quantum systems under frequency modulation, *Rep. Prog. Phys.* **80**, 056002 (2017).
- [3] P. Krantz, M. Kjaergaard, F. Yan, T. P. Orlando, S. Gustavsson, and W. D. Oliver, A quantum engineer's guide to superconducting qubits, *Appl. Phys. Rev.* **6** (2019).
- [4] S. Pirandola, U. L. Andersen, L. Banchi, M. Berta, D. Bunandar, R. Colbeck, D. Englund, T. Gehring, C. Lupo, C. Ottaviani, J. L. Pereira, M. Razavi, J. S. Shaari, M. Tomamichel, V. C. Usenko, G. Vallone, P. Villoresi, and P. Wallden, Advances in quantum cryptography, *Adv. Opt. Photon.* **12**, 1012 (2020).
- [5] J. M. Martinis, Qubit metrology for building a fault-tolerant quantum computer, *Npj Quantum Inf.* **1**, 15005 (2015).
- [6] R. Landauer, The noise is the signal, *Nature* **392**, 658 (1998).
- [7] R. J. Schoelkopf, A. A. Clerk, S. M. Girvin, K. W. Lehnert, and M. H. Devoret, Qubits as spectrometers of quantum noise, in *Quantum Noise in Mesoscopic Physics*, Quantum Noise in Mesoscopic Physics. NATO Science Series, Vol. 97, edited by Y. V. Nazarov (2003) pp. 175–203.
- [8] S. Danilin, A. Lebedev, A. Vepsäläinen, G. B. Lesovik, G. Blatter, and G. S. Paraoanu, Quantum-enhanced magnetometry by phase estimation algorithms with a single artificial atom, *Npj Quantum Inf.* **4**, 29 (2018).
- [9] A. R. Shlyakhov, V. V. Zemlyanov, M. V. Suslov, A. V. Lebedev, G. S. Paraoanu, G. B. Lesovik, and G. Blatter, Quantum metrology with a transmon qutrit, *Phys. Rev. A* **97**, 022115 (2018).
- [10] N. N. Gusarov, M. R. Perelshtein, P. J. Hakonen, and G. S. Paraoanu, Optimized emulation of quantum magnetometry via superconducting qubits, *Phys. Rev. A* **107**, 052609 (2023).
- [11] P. Szańkowski, G. Ramon, J. Krzywda, D. Kwiatkowski, and L. Cywiński, Environmental noise spectroscopy with qubits subjected to dynamical decoupling, *J. Phys. Condens. Matter* **29**, 333001 (2017).
- [12] J. Bylander, S. Gustavsson, F. Yan, F. Yoshihara, K. Harrabi, G. Fitch, D. G. Cory, Y. Nakamura, J.-S. Tsai, and W. D. Oliver, Noise spectroscopy through dynamical decoupling with a superconducting flux qubit, *Nat. Phys.* **7**, 565 (2011).
- [13] M. Jerger, A. Kulikov, Z. Vasselin, and A. Fedorov, In situ characterization of qubit control lines: A qubit as a vector network analyzer, *Phys. Rev. Lett.* **123**, 150501 (2019).
- [14] R. Harper, S. T. Flammia, and J. J. Wallman, Efficient learning of quantum noise, *Nat. Phys.* **16**, 1184 (2020).
- [15] F. Wudarski, Y. Zhang, A. N. Korotkov, A. Petukhov, and M. Dykman, Characterizing low-frequency qubit noise, *Phys. Rev. Appl.* **19**, 064066 (2023).
- [16] A. Youssry, G. A. Paz-Silva, and C. Ferrie, Noise detection with spectator qubits and quantum feature engineering, *New J. Phys.* **25**, 073004 (2023).
- [17] A. V. Lebedev, G. B. Lesovik, and G. Blatter, Optimal noninvasive measurement of full counting statistics by a single qubit, *Phys. Rev. B* **93**, 115140 (2016).
- [18] T. T. Heikkilä and T. Ojanen, Quantum detectors for the third cumulant of current fluctuations, *Phys. Rev. B* **75**, 035335 (2007).
- [19] S. Dogra, J. J. McCord, and G. S. Paraoanu, Coherent interaction-free detection of microwave pulses with a superconducting circuit, *Nat. Commun.* **13**, 7528 (2022).
- [20] J. J. McCord, S. Dogra, and G. S. Paraoanu, Theory of coherent interaction-free detection of pulses, *Phys. Rev. Res.* **5**, 033012 (2023).
- [21] G. S. Paraoanu, Interaction-free measurements with superconducting qubits, *Phys. Rev. Lett.* **97**, 180406 (2006).
- [22] G. S. Paraoanu, Generalized partial measurements, *EPL (Europhysics Letters)* **93**, 64002 (2011).
- [23] G. S. Paraoanu, Partial measurements and the realization of quantum-mechanical counterfactuals, *Found. Phys.* **41**, 1214 (2011).
- [24] J. Bell, T. H., Representation of random noise by random pulses, *Journal of Applied Physics* **45**, 1902 (2003), ht.
- [25] W. Belzig, Full counting statistics in quantum contacts, in *CFN Lectures on Functional Nanostructures Vol. 1: Vol. 1*, edited by K. Busch, A. Powell, C. Röthig, G. Schön, and J. Weissmüller (Springer Berlin Heidelberg, Berlin, Heidelberg, 2005) pp. 123–143.
- [26] M. Cattaneo and G. S. Paraoanu, Engineering dissipation with resistive elements in circuit quantum electrodynamics, *Adv. Quantum Technol.* **4**, 2100054 (2021).